JOURNAL OF SPACECRAFT AND ROCKETS
Vol. 44, No. 3, May–June 2007

Slender Solar Sail Booms: Finite Element Analysis

Ilinca Stanciulescu,* Lawrence N. Virgin,† and Tod A. Laursen‡
Duke University, Durham, North Carolina 27708

DOI: 10.2514/1.20526

Various aspects related to the numerical (finite element) analysis of the support structure for solar sails are analyzed. Static analyses of single booms (simple beam and isogrid configurations) are presented and dynamic properties are extracted before and beyond the buckling load. Numerical difficulties associated with the case of buckling under nonconservative loading are also explored using as a reference example von Beck's problem, for which a closed-form solution for comparison is available. A study of the entire support structure for a square solar sail (four connected booms) is also presented. In all analyses, attention is focused on the prediction of the postbuckling (large deflection) behavior, including dynamics.

I. Introduction

SOLAR sails offer the prospect of an effective propulsion system for deep space exploration using the energy from photon fluxes. Advances in lightweight materials, especially, have led to consideration of various geometries and configurations designed to harness the sun photons. Square, circular, or heligyro configurations have been proposed (see Fig. 1). The structural behavior of the solar sail is being analyzed from different perspectives (experimental, numerical, etc.) by various researchers (to mention only few of the studies, see, for instance, [1–4].)

To provide an appropriate surface to capture this solar effect, the sail must be supported in its deployed (or operational) state in the same way that a kite is supported by a relatively rigid framework. The key components of the support structure for solar sails are the slender booms, which are able to carry the axial and lateral loads to which they are subjected and can maintain the geometric configuration of the sail. Given the need to minimize weight, these booms tend to be somewhat slender, and hence buckling and vibration problems become an important issue. The booms must also have a reduced launch volume; that is, they must have the ability to be folded. Consequently, the material must be able to withstand high strain rates and must have a good shape memory function for the deployment sequence to be successful. Different structural configurations include the possibility of using inflatable members and various composite materials. There are also different choices available for the attachment of the sail membrane to the booms. Some of the possible solutions and their advantages and disadvantages are discussed in [5] and are shown in Fig. 2. Essentially, the determining factor influencing the static and dynamic postbuckling behavior of these slender structural elements is the way in which the load is transferred from the membrane to the boom.

The work described in this paper focuses on some aspects of the static and dynamic analysis of such structures; corresponding numerical examples are presented. Much of this work is based on finite element analysis considering complicated effects associated with large deflections, geometric imperfections, and transient dynamics. Because experimental testing of full-scale models including the characteristics of the environment in which they will be used (no gravity and practically no damping) is almost impossible, high confidence in the numerical models that are used has to be acquired.

Two different structural designs of the booms are analyzed. The first design considered is, from the numerical model point of view, just a regular beam. The second is the isogrid configuration, practically a 3-D trusslike structure often encompassing some kind of inflated interior for added stiffness and deployment. For a detailed description of the geometry, see [6,7]. In the case of the isogrid boom, high modulus fibers are oriented longitudinally and designed to absorb the compressive loads, whereas the ones oriented laterally absorb the inflation loads and stabilize the cross section. The fibers are impregnated with a Sub Tg resin to rigidize the structure after deployment. There are different isogrid configurations that have been considered for the solar sail booms. The mesh for the particular configuration that was used in this study was generated according to the geometry described in [7] and is shown in Fig. 3. The baseline model considered in this paper is a cantilever beam that has 16 circumferential bays (distributed uniformly on a circle of diameter 17.78 cm) and a helix that wraps around; the individual bars have a diameter of 5 mm. The total length corresponds to 100 full helices; that is, $L = 32.04$ m, the structure thus having a very high slenderness ratio. For validation purposes, this isogrid structure is also analyzed in [8], in which the authors, by means of a combination of ground testing and simplified analysis, show this ultralightweight boom to be scalable, predictable, and thermomechanically stable. The work presented in Secs. II and III of our paper approaches the analysis of the isogrid from the numerical perspective, but has the same goal: to efficiently predict the on-orbit performance of these modern ultralight structures. Section IV follows with an analysis of the numerical difficulties associated with the case of nonconservative loading. The paper ends with Sec. V discussing the complete support structure.

In a standard "structural engineering" approach, it is frequently assumed that buckling represents structural failure. What is unusual about the solar sail booms is that in this case we rely on a totally different design concept. Not only are buckled configurations accepted as operational in this case, but sometimes the structure is designed to buckle. Buckled booms have certain advantages in this case. First, they allow for configurations in which the sail is guaranteed to be in tension, thus satisfying the geometric requirement. Then, if the booms are allowed to buckle, they can be made slender and therefore lighter, which is favorable not only for vehicle efficiency but also for the costs associated with launching the structure into space. And last but not least, in the vicinity of buckling, a structure has lower natural frequencies, thus favoring structural control.

Various structural systems were analyzed in our study and different ways of transmitting the loads from the sail to the beams were explored. In this paper only directly applied forces are considered. The interested reader is referred to [9], in which the case

Received 14 October 2005; revision received 27 February 2006; accepted for publication 18 December 2006.

*Postdoctoral Research Associate, Department of Civil and Environmental Engineering; currently Assistant Professor, Department of Civil and Environmental Engineering, University of Illinois at Urbana–Champaign, Urbana, IL 61801. Member AIAA.

†Professor, Department of Mechanical Engineering and Materials Science. Member AIAA.

‡Professor, Department of Civil and Environmental Engineering.

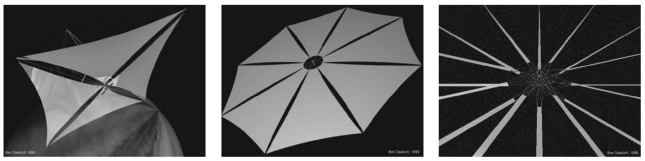

a) Square sail b) Circular sail c) Heligyro

Fig. 1 Structural configurations for solar sails (images created by Benjamin Diedrich, courtesy of www.solarsails.info).

of an indirectly transmitted force was considered. In this case, the system of cables used for keeping the sail integrity is at the same time the means through which the loading is transmitted to the booms, via cables that pull the tips of the cantilevers.

II. Large Deflection Static Analysis of a Single Boom

Various static and dynamic analyses are performed (using the finite element analysis software ABAQUS [10]) on both the standard beam and the isogrid configuration. In both cases, first-order, 3-D Timoshenko (shear-flexible) beam elements (B31) are used for discretization. These elements are formulated for large strains and large rotations, allow for transverse shear deformation, and are efficient for thick as well as slender beams. The discretizations used for both configurations are proved (via a spatial convergence study) to offer the desired accuracy.

As an example, in the case of the baseline model in the eigenvalue problem, a buckling load of $P_{\text{cr}} = 2.4736$ kN is obtained, a value that compares well with the analytical critical Euler load [11],

$$P_{\text{cr}} = \frac{\pi^2 EI}{4L^2} \tag{1}$$

The same configuration (see Fig. 3) is then loaded with a transverse load of 1% of the buckling load and a large deformation static analysis is performed with the aid of Riks's [12] continuation method. Among all path-following numerical techniques, the arc-length techniques are the ones known to perform well when special events (limit, bifurcation points) are encountered. In these cases, the historically prevalent approach (i.e., the load-controlled) is not robust with the analysis failing as soon as the limit or bifurcation point is encountered. Indeed, a load-controlled path-following approach fails here, whereas Riks's algorithm performs very well, and the structure is loaded up to approximately twice the critical load. Figure 4 presents the load-deflection diagram obtained from this analysis (u_1, u_2, and u_3 are the deflections at the free end in the x, y, and z directions), whereas the deformed configuration corresponding to the maximum compressive load that was applied (5 kN) is shown in the inset. These deformations are excessive, extending well beyond the expected range of design configurations for a solar sail boom, and are included here mainly to assess the capabilities of the finite element software. Analytical solutions rarely exist for highly nonlinear problems, but in this case such a solution is available (the so-called elastica solution [11], based on the "exact" differential equation in arc-length coordinates) and it is used here for comparison. These points are represented in Fig. 4 with square markers and their coordinates denoted with superscript "e." As can be seen, a very good match is obtained between the numerical model and the exact solution.

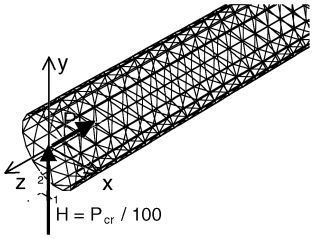

Fig. 3 Isogrid configuration.

This analysis was repeated using a simplified beam (a cantilever beam with a constant cross section). The cross-sectional properties of this equivalent beam were evaluated to be averages of the properties of the isogrid system. It has been confirmed that for slender elements, an analysis using an equivalent beam is very accurate and much more efficient.

III. Dynamic Analysis of a Single Boom

The dynamic analysis confirms the expectation that isogrid beams with high slenderness ratios present the same dynamic behavior as the long beams. The lower modes are bending modes as expected. The variation of the lowest four frequencies with the axial load is presented in Fig. 5, and two of the modal shapes (corresponding to the unloaded beam) are shown in the corresponding insets. The modes appear in pairs corresponding to the two principal directions of the cross section.

The prediction of the dynamic response of space structures in postbuckled and/or large deflection configurations is an important aspect of an adequate structural design. Furthermore, for effective control, the frequencies of vibration about highly deflected equilibria need to be known (especially important because of the lack of damping in space). The next step of the study analyzes, therefore, the variation of the natural frequencies with the axial load (which was increased from zero to approximately twice the critical load). As can be seen in Fig. 5, the lower bending modes present the same behavior (the continuous lines correspond to modes obtained during an analysis with a transverse load of $H = P_{\text{cr}}/100$, and the dashed lines correspond to the geometrically perfect system under pure axial loading). Because the transverse load represents a break in the system's symmetry, it is not surprising that the pair separates after buckling in that case. For the symmetric case, the modes remain identical in the two principal directions, the solution obtained in this case being the unstable branch (i.e., the nonbuckled configuration).

Figure 6 presents the expected decrease of the natural frequencies with the slenderness ratio of the beam defined as

$$\frac{L}{r} = \frac{L}{\sqrt{I/A}} \tag{2}$$

where L is the length of the beam, I and A are the cross-sectional inertia moment and area, and r is the radius of gyration. The lowest four vibration frequencies are represented in this figure. For comparison purposes, an analytical estimate of the fundamental frequency is included,

$$\omega_1 = (1.875)^2 \sqrt{\frac{EI}{mL^4}} \tag{3}$$

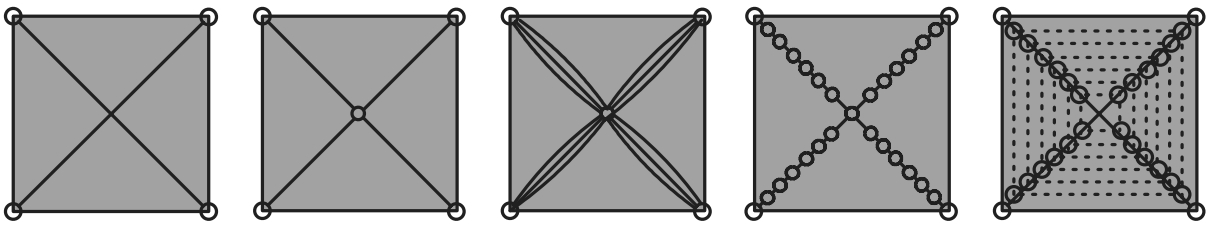

a) Four point suspension b) Five point suspension c) Separate quadrants d) Continuous connection e) Stripped architecture

Fig. 2 Sail attachment solutions.

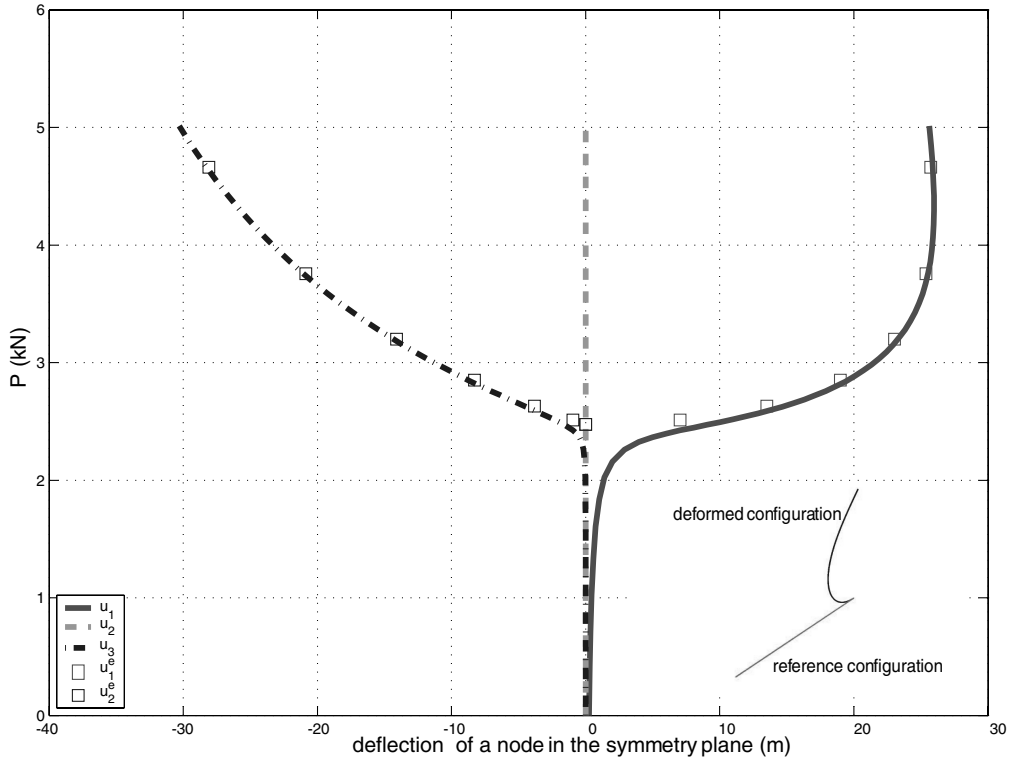

Fig. 4 Load-deflection diagram obtained with Riks' method [12] on baseline isogrid model.

with EI the cross-sectional flexural rigidity, m the mass per unit length, and L the total length of the beam. These properties were estimated in an average sense. Equation (3) gives the smallest solution of the eigenvalue problem for beams in bending and from Fig. 6 it can be seen that good agreement is obtained with the numerically evaluated ones. The same good agreement is observed for the higher frequencies as well, which can be computed analytically via

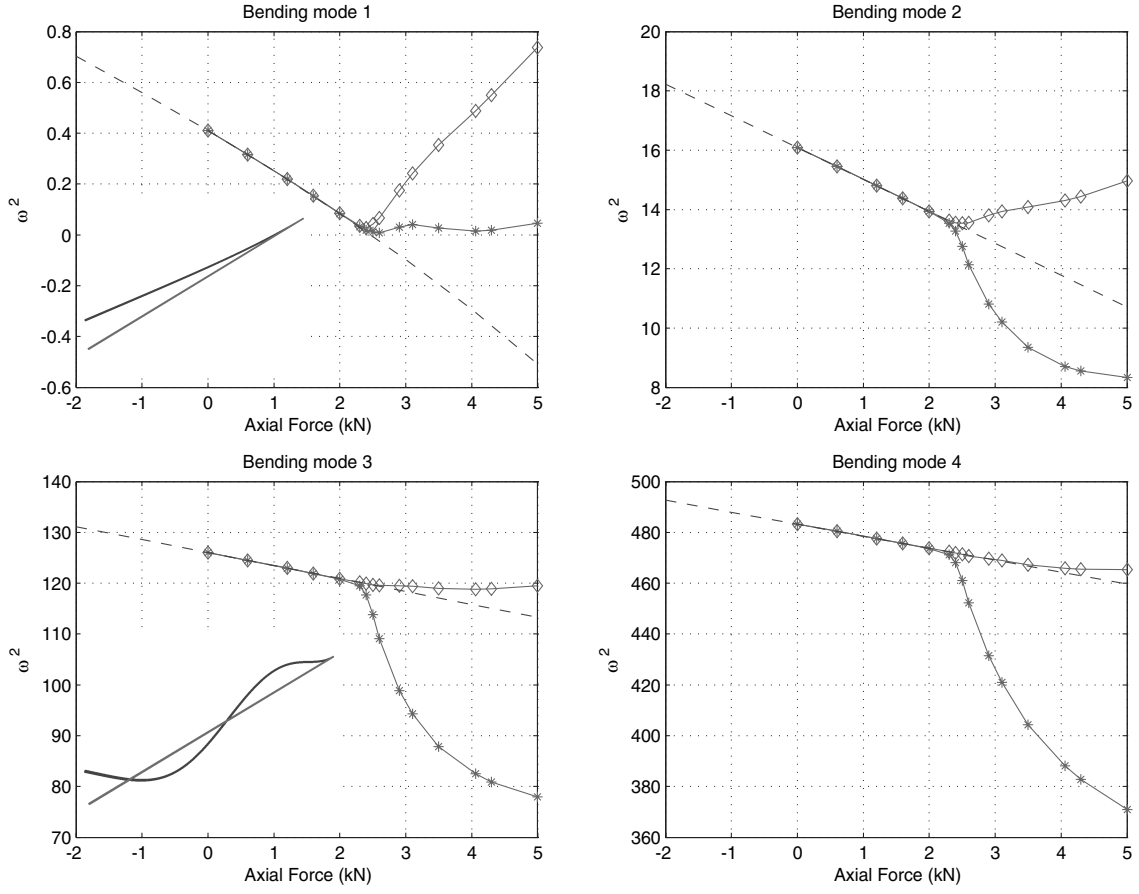

Fig. 5 Variation of the square of the natural frequencies with the axial loading.

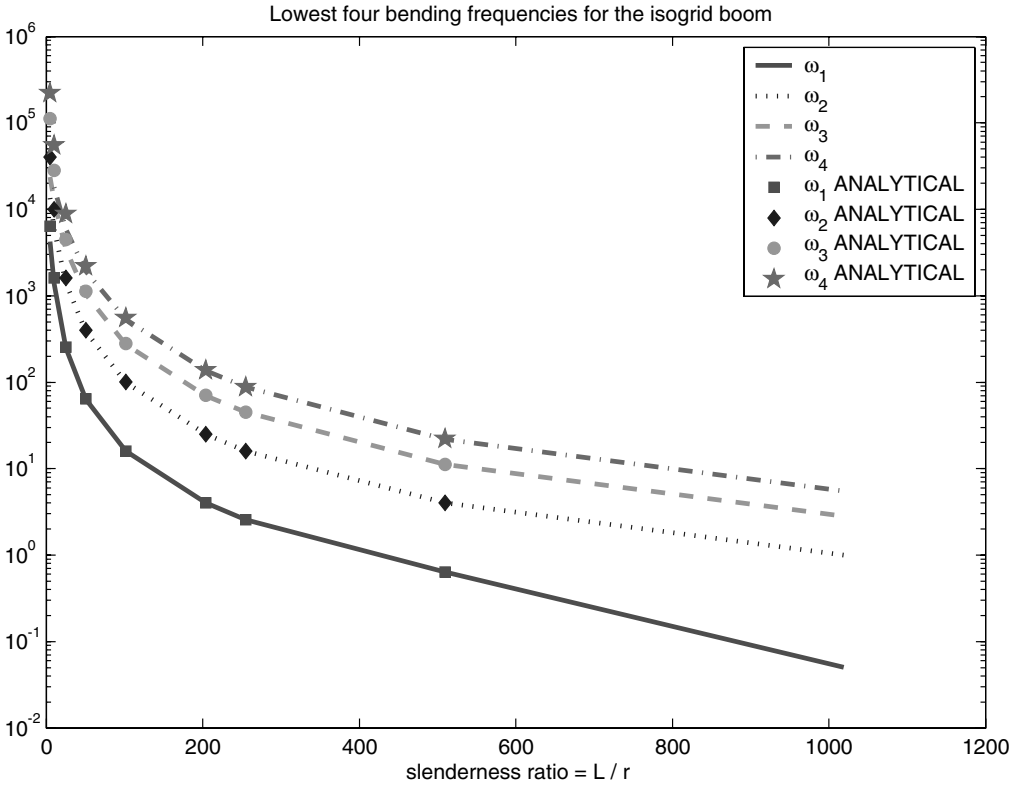

Fig. 6 Variation of the natural frequencies with the slenderness ratio.

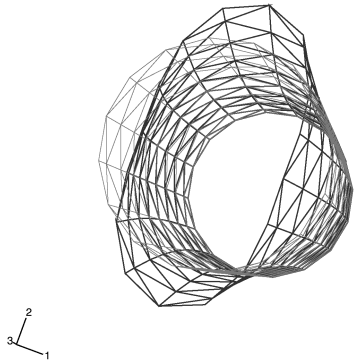

Fig. 7 Buckling mode of a short isogrid.

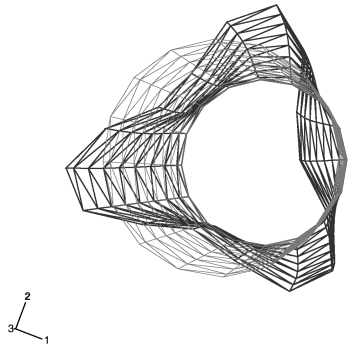

Fig. 8 Vibration mode of a short isogrid.

$$\omega_2 = (4.694)^2\sqrt{\frac{EI}{mL^4}}, \qquad \omega_3 = (7.855)^2\sqrt{\frac{EI}{mL^4}}$$
$$\omega_4 = \left(\frac{7\pi}{2}\right)^2\sqrt{\frac{EI}{mL^4}} \tag{4}$$

In all dynamic analyses that are performed, the occurrence of longitudinal and circumferential modes is also observed. For large overall dimensions (i.e., very long slender booms) these modes are not important (they represent higher modes). However, the sail attachments provide constraints and thus may considerably shorten the effective lengths. In the case of the very small slenderness ratios (relatively stocky beams), the behavior is considerably different. Both the buckled configuration (see Fig. 7) and the lowest vibration modes (Fig. 8) have a significant circumferential component. Qualitatively these buckling and vibration modes are similar to modes corresponding to thin cylindrical shells [13] with various numbers of circumferential and axial waves. Although such modes exist in the longer isogrid booms as well, in that case they are higher modes, and the range of lower modes is dominated by beamlike bending eigenshapes.

For long slender isogrid booms, the use of an equivalent beam model for the analysis leads to increased numerical efficiency and is capable of recovering most of the results obtained on the complex isogrid model. Both the evaluation of the buckling load as well as the modal analysis return satisfactory results based on this simplified model. A comparison of the results is shown in Fig. 9 for the vibration mode pairs 1, 2, and 7.

A very good agreement is obtained for lower modes and relatively low axial loading. Some differences are observed in the higher modes and in the postbuckled state, but even in this case the relative error is small and the behavior is quite well predicted by a very simple model that recovers the lowest (bending) modes with good accuracy.

Another application that is of interest considers the case of long slender booms with intermediate supports. There are several choices for the suspension of the sail [6]. A stripped architecture or continuous connections bring additional sail attachment points, and the numerical model has to take into account the effect of these lateral constraints. The buckling load and the natural frequencies corresponding to bending modes for this case increase with the increase in the number of lateral supports (i.e., with the reduction of the effective length), whereas the longitudinal modes remain, as expected, unchanged by any modification in the lateral conditions.

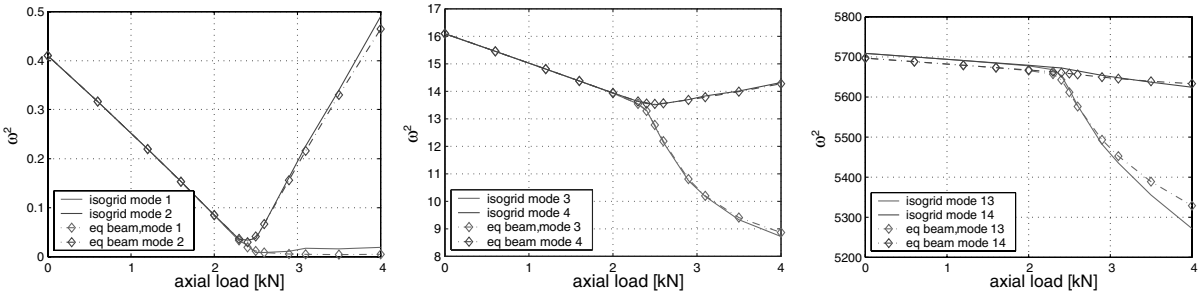

a) First bending mode **b) Second bending mode** **c) Seventh bending mode**

Fig. 9 Comparisons of various bending mode frequencies; analysis of isogrid and equivalent beam.

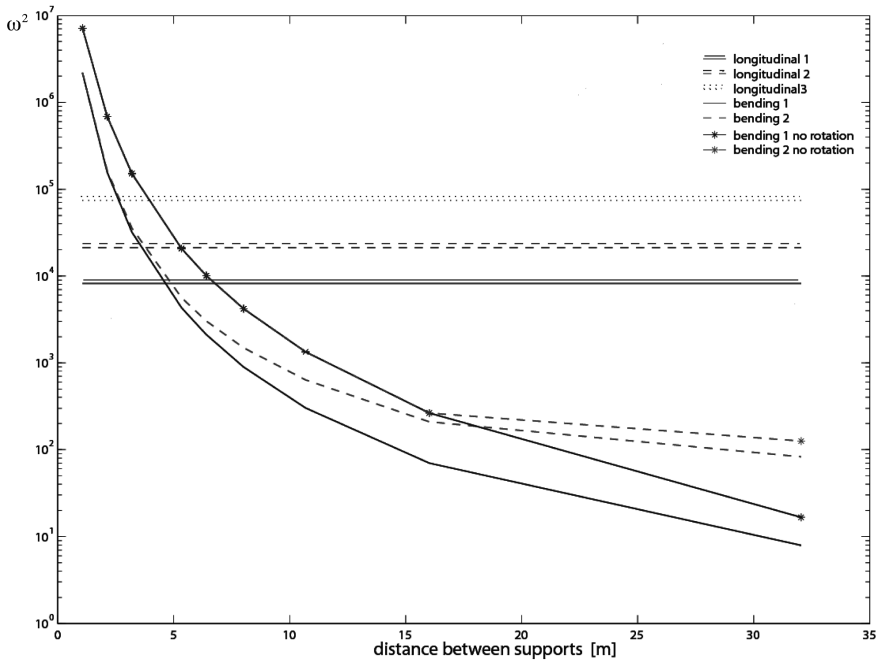

Fig. 10 Variation of the square of the natural frequencies with the distance between supports.

Figure 10 shows the variation of the natural frequencies with the distance between the supports and the nature of these supports. We considered two cases: free or restrained rotation at the supports. Because the model with intermediate supports is motivated by the designs with intermediate sail attachments, the more realistic one is probably the free-rotation version. The effect of the lateral supports on all modes is studied and, as expected, longitudinal modes are not affected.

IV. Buckling Under Nonconservative Forces

If the system's loading is nonconservative, the loss of stability may not occur via static buckling (the system evolving towards another equilibrium state) but by the system going into an unbounded motion. To be able to analyze this case, dynamic effects must be considered, stability being essentially a dynamic concept. The problem of the cantilever beam under a tip follower force was first dealt with in a dynamic context by Max von Beck in 1952 [14], who proved that buckling in this case is intrinsically dynamic, and not including the time in an analysis will result in an erroneous conclusion. The buckling load in the case of a constant-direction force P can be evaluated statically [11] and for a cantilever beam is

$$P_{\text{cr}} = \frac{\pi^2 EI}{4L^2} \tag{5}$$

In the case of the *follower* force P, the vertical component of the load (denoted by P^v) at buckling is approximately 8 times higher than this, as will be shown later. The x direction is the undeformed beam axis. In a more general context this problem was also studied by Bolotin [15]. Although the case of the follower force is not directly applicable to the problem discussed in this paper, other nonconservative load configurations (for instance, subtangential loads) may be present in some of the structural systems used to describe solar sail booms. Understanding the numerical aspects associated with the analysis of this type of loading is important and for this purpose von Beck's problem [14] is used as an example.

Consider a cantilever beam with flexural rigidity EI, mass density ρ, length L, and cross-sectional area A (assumed constant over the length of the beam). It is noted here that the bending analysis neglects transverse shear deformation and rotary inertia. The Cartesian coordinate x is along the undeformed elastic beam centerline, and $y(\xi, t)$ denotes the deflection at time t of the section at $x = \xi$ (see Fig. 11).

The tip force can be resolved into its vertical and horizontal components (P^v and P^h) acting at the section at $x = L$ and the elementary inertia force at a current section can be calculated via

$$\mathrm{d}\,T(\xi) = \rho \ddot{y}(\xi, t) A \,\mathrm{d}\xi \tag{6}$$

The bending moment at current section (x) produced by the action of the inertia forces is

$$M_i(x) = \int_x^L \rho \ddot{y}(\xi, t) A(\xi - x)\,\mathrm{d}\xi \tag{7}$$

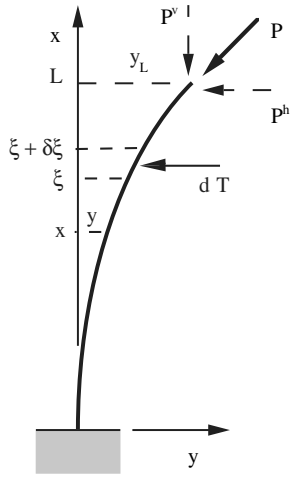

Fig. 11 Von Beck's problem [14].

and the differential equation of the beam can be written as

$$EI\frac{\partial^4 y}{\partial x^4} + P^v\frac{\partial^2 y}{\partial x^2} + \rho A\ddot{y} = 0 \tag{8}$$

The boundary conditions associated with this problem are

$$y(0,t) = 0, \qquad \left.\frac{\partial y}{\partial x}\right|_{(0,t)} = 0, \qquad \left.\frac{\partial^2 y}{\partial x^2}\right|_{(l,t)} = 0, \qquad \left.\frac{\partial^3 y}{\partial x^3}\right|_{(l,t)} = 0 \tag{9}$$

Assuming the solution can be expressed as

$$y(x,t) = A_0 e^{\lambda x} e^{i\omega t} \tag{10}$$

and using the notations $p = P^v/EI$ and $a = \rho A/EI$, the characteristic equation is obtained

$$\lambda^4 + p\lambda^2 - a\omega^2 = 0 \tag{11}$$

that has the solutions [14] $\pm\lambda_1$ and $\pm i\lambda_2$, where

$$\lambda_1 = \sqrt{\frac{\sqrt{4a\omega^2 + p^2} - p}{2}} \tag{12}$$

$$\lambda_2 = \sqrt{\frac{\sqrt{4a\omega^2 + p^2} + p}{2}} \tag{13}$$

A comment should be made here on the indispensability of including the time component in the solution. It can be seen that ignoring the dynamic component [i.e., $\omega = 0$ in Eq. (10)] results in $p = 0$, and thus the trivial solution only is obtained. Because this would appear to be the only solution and no neighboring equilibria could be found, one would mistakenly have concluded that the trivial solution never loses stability. The dynamic buckling load (obtained numerically) from the eigenvalue problem is

$$P^v_{\text{cr}} = \frac{20.1EI}{L^2} \tag{14}$$

and was computed using Mathematica.

A dynamic analysis is performed with ABAQUS for this problem and shows an oscillatory response after buckling (as seen in Fig. 12). In Fig. 13, a set of screen snapshots at different times present the evolution of the deformed shape during this analysis. A spatial convergence study performed in this case exposed a surprising effect: the number of elements required in this analysis is much larger than what proves to be more than sufficient in the case of the static analysis. All subsequent results are obtained based on these very refined discretizations.

From the numerical point of view, one can sometimes simplify the analysis of instabilities by using either a static arc-length algorithm or a numerically more efficient approach, namely, a static analysis with numerical damping included (to avoid algorithmic instabilities). However, these methods do not perform well when the instabilities are dynamic in nature. For instance, in the case of von Beck's problem [14], the Riks (arc-length) algorithm [12] is not able to follow the loading path beyond the buckling. Including numerical damping in the model makes the analysis more stable, but the artificial viscous forces included in the system are locally significant and alter the results (see Fig. 14). Even though the numerical damping is very small (characterized by a coefficient of 10^{-6}), the buckling load predicted using this type of analysis is almost twice the exact value. We conclude that in cases like this, a dynamical analysis is required.

Because the analysis failed soon after the onset of the oscillatory behavior, the inclusion of the numerical damping in the dynamic simulation was also tested but did not seem to offer any advantages.

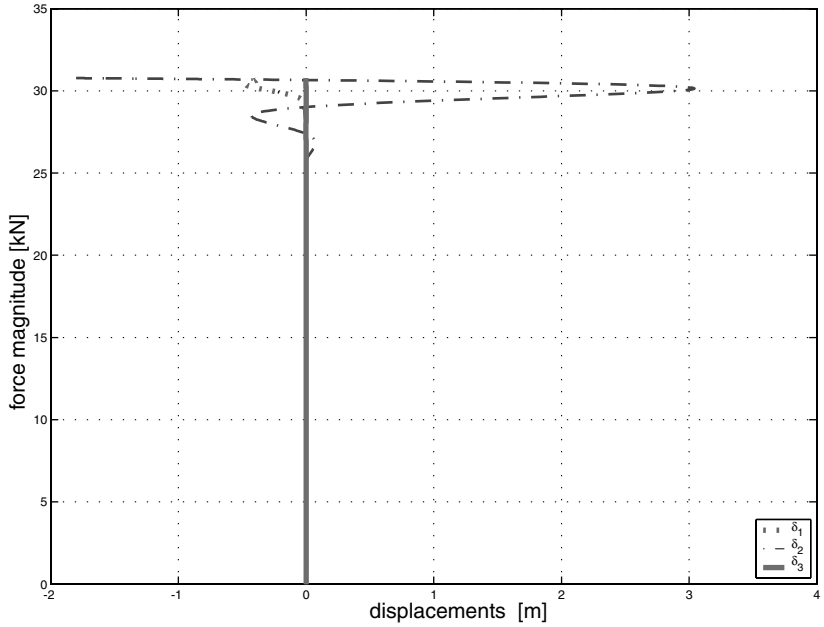

Fig. 12 Dynamic analysis of von Beck's problem [14] using ABAQUS.

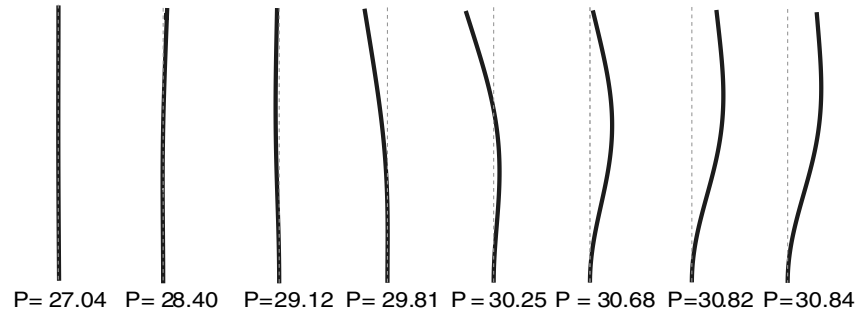

Fig. 13 Evolution of the deformation during a dynamic analysis with ABAQUS. Load values are in kN and are linearly related to time.

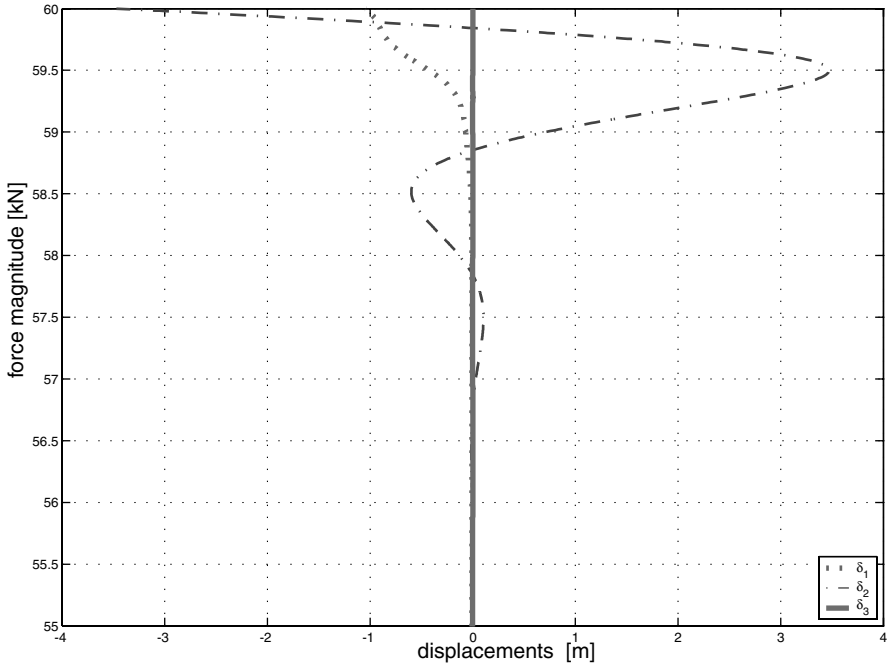

Fig. 14 Static analysis of von Beck's problem [14] using ABAQUS; numerical damping included in an attempt to control algorithmic instabilities.

Results were strongly dependent on the amount of damping, and the analysis did not extend much above the failure limit for the case with zero damping as seen in Fig. 15. It appears that local effects are too important in this case and inclusion of any artificial damping factors is not beneficial.

V. Analysis of the Four-Boom Structure for a Square Sail

This section analyzes a support structure of a square sail composed of four booms (all identical with the equivalent beam model

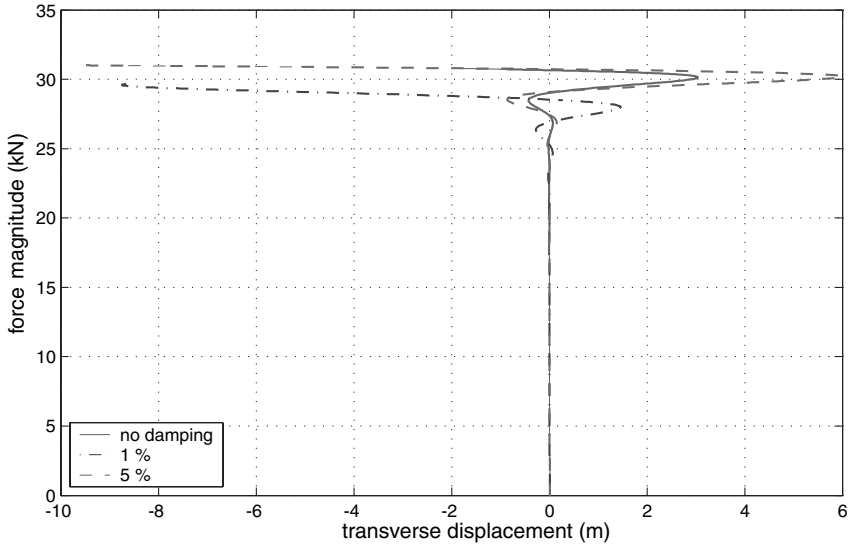

Fig. 15 Dynamic analysis of von Beck's problem [14] using ABAQUS; numerical damping included.

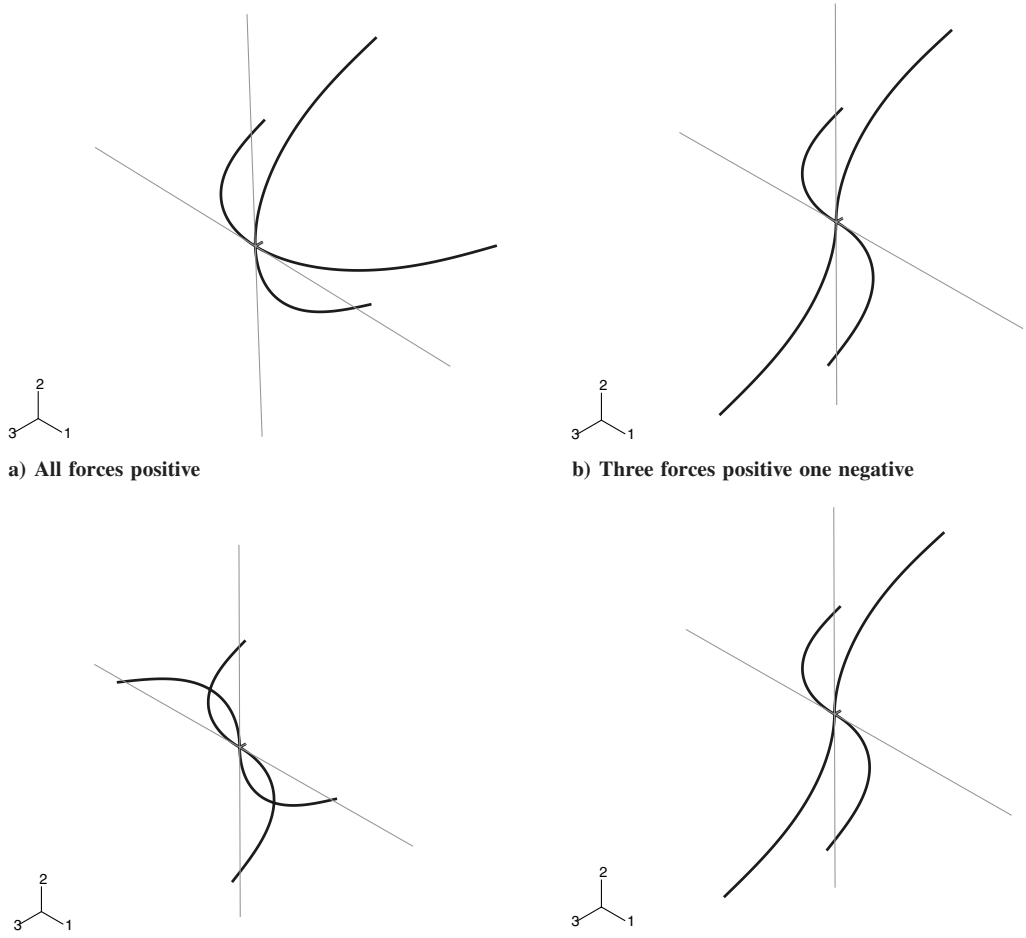

a) All forces positive

b) Three forces positive one negative

c) Two forces positive and two negative (symmetric)

d) Two forces positive and two negative (antisymmetric)

Fig. 16 Structural deformed configurations under various combinations of lateral forces. Compressive axial forces of 3 kN in all beams.

presented in Sec. III) fixed on a central support, a short and rigid cantilever beam. The static and dynamic behavior of this structure was analyzed under axial loading similar with the loading used in Secs. II and III. The buckling load and the natural frequencies corresponding to this system are almost identical with those calculated in the case of the single boom. The effect of the rigidity of the central support was studied by increasing its flexural rigidity by a factor of 5 and 10, respectively. As expected, the larger the rigidity, the better the match with the predictions for the single boom. The large deflection static analysis was performed with Riks' algorithm [12] and the load-deflection diagrams that were obtained for the tips of the booms are similar to Fig. 4. The full supporting structure not only keeps the same symmetry of the cross section with respect to its principal inertia axis, but also brings new symmetries with respect to the global structural axis. As a consequence, the order of multiplicity of the eigenvalues is increased, the spectrum has not just a pair of identical eigenvalues that will split after buckling, but instead a larger set of eigenvalues corresponding to each bending mode.

Small lateral forces applied at the tips of the four booms give the initial imperfection, similar to the approach used in the analysis of the single boom. However, in the model of the full structure, various configurations have been considered: 1) all four lateral forces in the same direction (all positive); 2) three positive, one negative; 3) two positive, two negative (symmetric with respect to the central point); and 4) two positive, two negative (asymmetric). The deformed configurations obtained in these cases are shown in Fig. 16. Depending on the stiffness of various components of the structure and on the values of the initial imperfections, the final deformed geometry favors either a symmetric (16a and 16c) or an antisymmetric (16b and 16d) configuration.

The variation of the natural frequencies with the axial load for the base model (flexural rigidity of the central support $= K$) is presented in Fig. 17, in which the four different symbols represent each of the four configurations of the initial imperfection described earlier.

It can be seen that with the exception of the increased number of eigenvalues corresponding to the same type of eigenmode and of slight differences in this *repeated eigenvalue*, there is no fundamental difference between the structural behavior and the behavior of the single boom. Because of the specific geometry and the many symmetries involved, the lower structural vibration modes are nothing but *multiplicative* representations of the modes of the single boom. The relative deviation of these coexisting solutions from the "average" value is small, even in the case of smaller rigidity of the central support stays below a 5% variation.

For comparison, we also show here the case corresponding to a central support with a flexural rigidity of 10 K (see Fig. 18), in which a better match is observed with the values predicted by the single boom analysis, at least up to loads in the vicinity of buckling. In the limit ($K \to \infty$), all four booms have the independent behavior of a cantilever beam and the plots from Fig. 5 are exactly recovered.

VI. Conclusions

For all the design models analyzed so far, complex effects such as strong geometric nonlinearities and large compressive forces were taken into account successfully. Vibration modes have been followed up to almost twice the critical load, along a loading path that was followed successfully with the aid of Riks' algorithm [12]. It was also shown that simpler equivalent beam models can effectively replace and predict the response of the slender isogrid booms with a considerable reduction of the number of degrees of freedom and hence an improvement in numerical efficiency. The same statement is no longer true for booms with shorter effective lengths (spans) and current work is concentrated on developing simpler equivalent

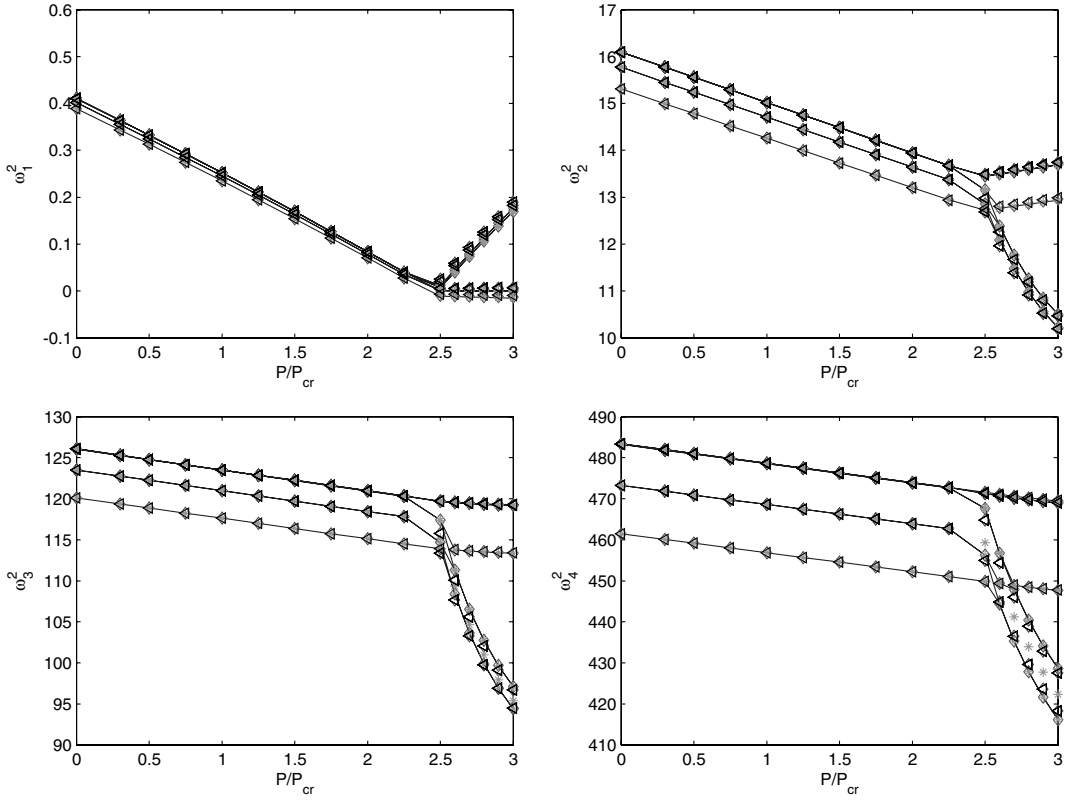

Fig. 17 Variation of the square of the natural frequencies with the axial loading (central support rigidity = 1 K).

models for this case. Dynamic analyses were used to predict the loss of stability for the case of nonconservative forces and the results are consistent with the analytical solutions for the simple case of the cantilever beam. Although the deflections analyzed were typically computed for loads above anticipated design values, it is instructive to determine the extent to which solutions can be obtained. Furthermore, it has been suggested that, due to weight and control facets of solar sail design, carrying loads in the vicinity of underlying elastic critical load (which would clearly be undesirable in regular structural applications) is not unrealistic.

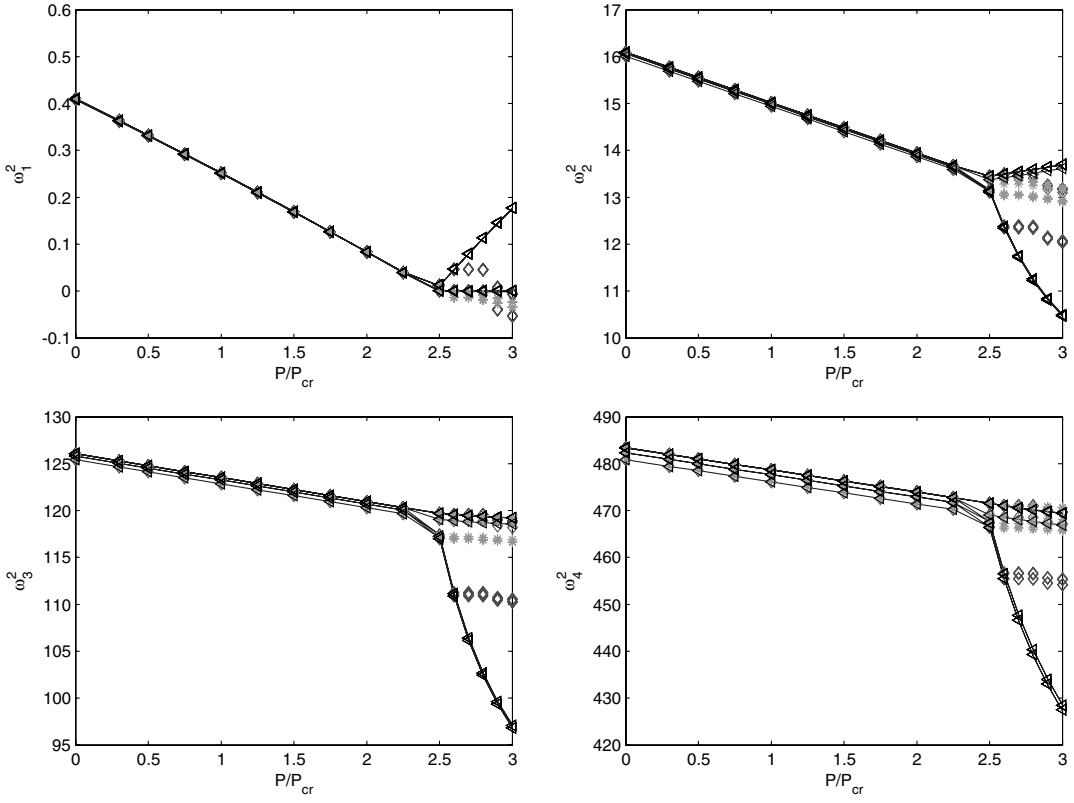

Fig. 18 Variation of the square of the natural frequency with the axial loading (central support rigidity = 10 K).

The behavior of a supporting structure composed of four identical booms is very similar to the behavior of a single boom. The next step of this study will be to perform dynamic analyses of full-scale models (considering also the inclusion of the sail), as well as verification with experimental data.

Acknowledgments

The work described in this paper was funded in whole or in part by the In-Space Propulsion Technology Program, which is managed by NASA's Science Mission Directorate in Washington, D.C., and implemented by the In-Space Propulsion Technology Office at Marshall Space Flight Center in Huntsville, Alabama. The program objective is to develop in-space propulsion technologies that can enable or benefit near and midterm NASA space science missions by significantly reducing cost, mass, or travel times. The specific contract was administered by NASA Langley Research Center under the program Research Opportunities in Space Science (ROSS) 2002 Cycle II In-Space Propulsion Technology NRA (ROSS-2002, NRA-OSS-01-ISPT2, SUBTOPIC 6.2).

References

[1] Greschik, G., and Mikulas, M. M., "Design Study of a Square Solar Sail Architecture," *Journal of Spacecraft and Rockets*, Vol. 39, No. 5, 2002, pp. 653–661.

[2] Pappa, R. S., Lassiter, J. O., and Ross, B. P., "Structural Dynamics Experimental Activities in Ultra-Lightweight and Inflatable Space Structures," *Journal of Spacecraft and Rockets*, Vol. 40, No. 1, 2003, pp. 15–23.

[3] Wang, J. T., and Johnson, A. R., "Deployment Simulation of Ultra-Lightweight Inflatable Structures," AIAA Paper 2002-1261, 2002.

[4] Yang, B., Lou, M., and Fang, H., "Buckling Analysis of Long Booms with Initial Geometric Imperfections," AIAA Paper 2004-1735, April 2004.

[5] Murphy, D. M., and Murphey, T. W., "Scalable Solar Sail Subsystem Design Considerations," AIAA Paper 2002-1703, 2002.

[6] Lichodziejewski, D., Derbes, B., West, J., Reinert, R., Belvin, K., and Pappa, R., "Bringing an Effective Solar Sail Design Toward TRL 6," AIAA Paper 2003-4659, 2003.

[7] Lin, J. K. H., Sapna, G. H., Cadogan, D. P., and Scarborough, S. E., "Inflatable Rigidizable Isogrid Boom Development," AIAA Paper 2002-1297, 2002.

[8] Agnes, G. S., Abelson, R. D., Miyake, R., Lin, J. K. H., Welsh, J., and Watson, J. J., "Preliminary Analysis of the 30-m Ultraboom Flight Test Article," AIAA Paper 2005-1972, April 2005.

[9] Holland, D. B., Stanciulescu, I., Virgin, L. N., and Plaut, R. H., "Vibration and Large Deflection of Cantilevered Elastica Compressed by Angled Cable," *AIAA Journal* (to be published).

[10] ABAQUS Analysis User's Manual, Ver. 6.4, ABAQUS, Inc., Providence, RI, 2003.

[11] Timoshenko, S. P., and Gere, J. M., *Theory of Elastic Stability*, 2nd ed., McGraw–Hill, New York, 1961.

[12] Riks, E., "An Incremental Approach to The Solution of Snapping and Buckling Problems," *International Journal of Solids and Structures*, Vol. 15, No. 7, 1979, pp. 529–551.

[13] Leissa, A., *Vibration of Shells*, Scientific and Technical Information Office, NASA, 1973.

[14] von Beck, M., "Die Knicklast des einseitig eigenspannten, tangential gedrückten Stabes," *ZAMP*, Vol. 3, No. 3, May 1952, pp. 225–228.

[15] Bolotin, V., *Nonconservative Problems of the Theory of Elastic Stability*, The Macmillan Company, New York, translated from Russian ed., 1963.

D. Edwards
Associate Editor